DOI: 10.1021/ic100447m

Inorganic Chemistry
Article

Probing the Structure, Conformation, and Stereochemical Exchange in a Family of Lanthanide Complexes Derived from Tetrapyridyl-Appended Cyclen

Louise S. Natrajan,[†] Ntai M. Khoabane,[‡] Benjamin L. Dadds,[†] Christopher A. Muryn,[†] Robin G. Pritchard,[†] Sarah L. Heath,[†] Alan M. Kenwright,[*,‡] Ilya Kuprov,[*,‡,⊥] and Stephen Faulkner[*,†,§]

[†]*School of Chemistry, University of Manchester, Oxford Road, Manchester M13 9PL, U.K.,* [‡]*Department of Chemistry, University of Durham, South Road, Durham DH1 3LE, U.K., and* [§]*Chemistry Research Laboratory, University of Oxford, Mansfield Road, Oxford OX1 3TA, U.K.* [⊥]*Current address: Oxford e-Research Centre, 7 Keble Road, Oxford OX1 3QG, U.K.*

Received March 8, 2010

A series of lanthanide complexes have been synthesized from 1,4,7,10-tetrakis(2-pyridylmethyl)-1,4,7,10-tetraazacyclododecane. Crystallographic studies indicate that, in the solid phase, all of the lanthanide ions are 9-coordinate and are bound to eight N atoms from the donor ligand, with the ninth site being filled by a counterion or solvent molecule. In solution, time-resolved luminescence studies indicate that the luminescence exhibits contributions from two species corresponding to the nonhydrated and hydrated forms. The NMR spectra in protic media show the presence of two dominant isomers on the NMR time scale; furthermore, the spectra are very different from those obtained for 1,4,7,10-tetraazacyclododecane-*N*′,*N*″,*N*‴,*N*⁗-tetraacetic acid (DOTA) and its derivatives. The different forms of the complex undergo slow conformational and enantiomeric exchange in solution, which has been measured by NMR. The exchange path has been mapped out by density functional theory calculations and shows multiple metastable conformations (with respect to the dihedral angles of the cyclen ring). This contrasts with the established NMR behavior of DOTA complexes, which has been described by a two-state solution equilibrium.

Introduction

Lanthanide complexes are of considerable current interest owing to their application as magnetic resonance imaging (MRI) contrast agents[1] and as luminescent probes in cellular imaging[2] and bioassay.[3] Luminescence from the lanthanide ions is long-lived and can be separated from short-lived fluorescence by using time-gating techniques. This approach has been widely applied to improve signal-to-noise ratios and lower detection limits in bioassay and luminescence microscopy.[4] However, direct excitation of the lanthanide ions is notoriously difficult as a result of the Laporte forbidden nature of f−f transitions. This difficulty is commonly circumvented by using chromophores with high extinction coefficients to sensitize the formation of the lanthanide excited state.[5] Once formed, the lanthanide excited state can be quenched nonradiatively through coupling to nearby O−H and N−H oscillators.[5,6] To avoid this vibrational relaxation, encapsulating ligands are often used to exclude water molecules from the coordination sphere, thus improving the luminescence quantum yield and luminescence lifetime.[7] In the case of near-IR luminescence from neodymium and ytterbium, C−H oscillators also play a significant role in nonradiative deactivation of the lanthanide excited state, meaning that much shorter lifetimes are observed for these ions.[5,7]

1,4,7,10-Tetraazacyclododecane-*N*′,*N*″,*N*‴,*N*⁗-tetraacetic acid (DOTA) and its derivatives (Figure 1) are widely used as ligands for lanthanide ions, and their structure and spectroscopic properties are well researched.[1,8] They form complexes with a very high degree of kinetic and thermodynamic stability: $[Gd(DOTA)]^-$, with a pK_d of 28.5, is in clinical use as an

*To whom correspondence should be addressed. E-mail: a.m.kenwright@durham.ac.uk (A.M.K.), ilya.kuprov@oerc.ox.ac.uk (I.K.), stephen.faulkner@chem.ox.ac.uk (S.F.).

(1) (a) Merbach, A. E.; Toth, E. In *Comprehensive Coordination Chemistry*, 2nd ed.; Ward, M. D., Ed.; Elsevier: New York, 2004; Chapter 19, Vol. *9*. (b) Parker, D.; Dickins, R. S.; Puschman, H.; Crossland, C.; Howard, J. A. K. *Chem. Rev.* **2002**, *102*, 1977.

(2) (a) Hemilla, I. A. *Applications of fluorescence in immunoassay*; Wiley Interscience: New York, 1991. (b) Bunzli, J. C. G.; Comby, S.; Chauvin, A. S.; Vandevyer, C. D. B. *J. Rare Earths* **2007**, *25*, 257.

(3) (a) Beeby, A.; Clarkson, I. M.; Faulkner, S.; Botchway, S.; Parker, D.; Williams, J. A. G.; Parker, A. W. *J. Photochem. Photobiol. B: Biol.* **2000**, *57*, 83. (b) Charbonniere, L.; Ziessel, R.; Guardigli, M.; Roda, A.; Sabbatini, N.; Cesario, M. *J. Am. Chem. Soc.* **2001**, *123*, 2436. (c) Weibel, N.; Charbonniere, L. J.; Guardigli, M.; Roda, A.; Ziessel, R. *J. Am. Chem. Soc.* **2004**, *126*, 4888.

(4) (a) Chauvin, A. S.; Comby, S.; Song, B.; Vandevyer, C. D. B.; Thomas, F.; Bunzli, J. C. G. *Chem.—Eur. J.* **2009**, *13*, 9515. (b) Palsson, L. O.; Pal, R.; Murray, B. S.; Parker, D.; Beeby, A. *Dalton Trans.* **2007**, 5726.

(5) Faulkner, S.; Burton-Pye, B. P.; Pope, S. J. A. *Appl. Spectrosc. Rev.* **2005**, *40*, 1.

(6) Parker, D.; Williams, J. A. G. *J. Chem. Soc., Dalton Trans.* **1996**, 3613.

(7) (a) Faulkner, S.; Natrajan, L. S.; Perry, W. S.; Sykes, D. *Dalton Trans.* **2009**, 3890. (b) Gunnlaugsson, T.; Leonard, J. P. *Chem. Commun.* **2005**, 3114.

(8) (a) Aime, S.; Botta, M.; Ermondi, G. *Inorg. Chem.* **1992**, *31*, 4291. (b) Aime, S.; Botta, M.; Fasano, M.; Paula, M.; Marques, M.; Geraldes, C. F. G. C.; Pubanz, D.; Merbach, A. E. *Inorg. Chem.* **1997**, *36*, 2059.

Published on Web 07/27/2010

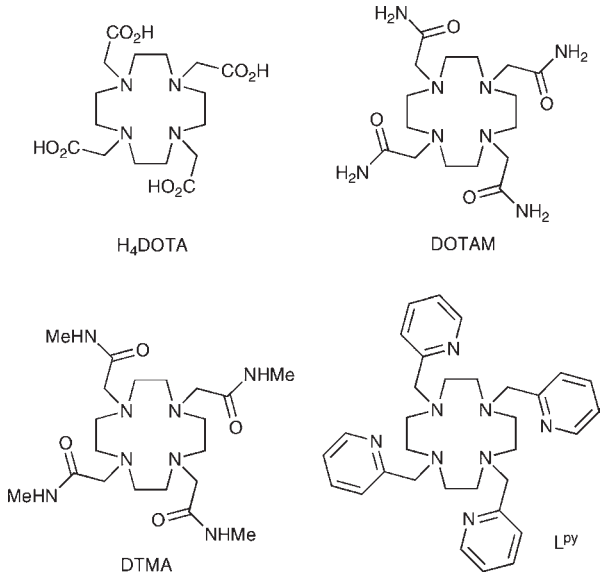

Figure 1. Tetrasubstituted cyclen derivatives.

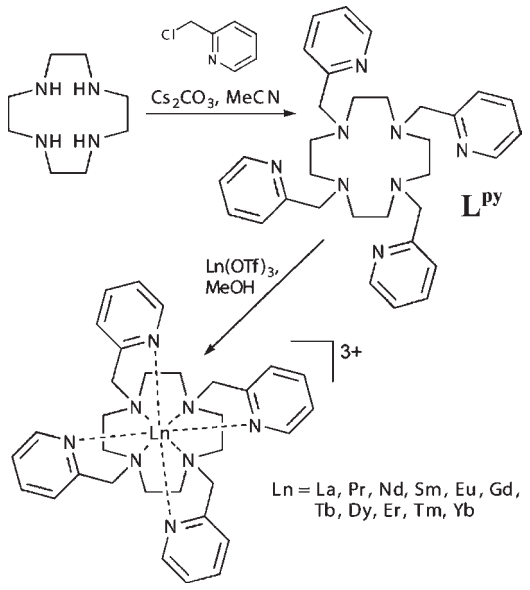

Figure 2. Synthetic pathway to L^{py} and its lanthanide complexes.

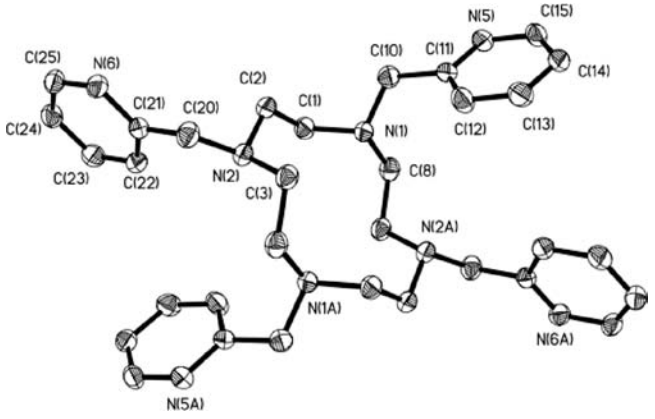

Figure 3. Thermal ellipsoid drawing of L^{py} (50%). H atoms are omitted for clarity. Selected distances (Å) and angles (deg): N(1)−C(1) 1.4692(14), N(2)−C(2) 1.4668(15), N(5)−C(11) 1.3376(15), N(6)−C(21) 1.3883; C(10)−N(1)−C(1) 109.91(9), C(2)−N(2)−C(3) 112.05(9), C(21)−N(6)−C(25) 117.05(11).

MRI contrast agent, and its dissociation in vivo has been estimated as having a half-life in thousands of years.

In this paper, we describe the synthesis of a family of complexes derived from 1,4,7,10-tetrakis(2-pyridylmethyl)-1,4,7,10-tetraazacyclododecane (L^{py}), which contains eight N atoms in its donor set and incorporates four pyridyl chromophores that can be used to sensitize metal-centered luminescence from a variety of lanthanides. The synthesis and crystallography of this ligand and its neodymium, europium, and terbium complexes have been reported independently by Nishihara et al.[9] In the current work, we compare our own crystallographic studies on a wider range of lanthanide metal complexes of the ligand (Pr, Nd, Eu, Gd, Tb, Er, and Yb) with the extensive literature for the well-known DOTA complexes and their derivatives and investigate the behavior of the complexes in solution by NMR and luminescence spectroscopy to study both the equilbrium structure of the complexes in solution and the pathways and mechanisms for exchange between isomers. Solution coordination isomerism of these complexes is investigated in detail using density functional theory (DFT), nuclear magnetic resonance (NMR), and time-resolved luminescence spectroscopy.

Results and Discussion

The parent ligand and its complexes were prepared as shown in Figure 2. The reaction of cyclen with 4 mol equiv of 2-(chloromethyl)pyridine and excess Cs_2CO_3 in acetonitrile yielded L^{py}, which was isolated in 87% yield as colorless blocks when recrystallized from acetonitrile. The ligand (its X-ray structure is shown in Figure 3) adopts an open, chair-like conformation analogous to that observed in many DOTA and DOTAM derivatives. The form of the product proved to be sensitive to the nature of the base used in the reaction; when sodium hydrogen carbonate was used in lieu of cesium carbonate, the product was isolated as a sodium chloride adduct $[L^{py}Na]Cl$.

Complexes were prepared by the reaction of L^{py} with the appropriate quantity of lanthanide triflate in methanol and purified by recrystallization from acetonitrile/diethyl ether. For complexes of the later metals in the lanthanide series (Er, Tm, and Yb), partial hydrolysis was observed in protic solvents, yielding the protonated ligand triflate adduct $[H_2L^{py}][OTf]_2$ and making it impossible to isolate analytically pure samples of the erbium, thulium, or ytterbium complexes, although their presence in a mixture with the protonated ligand was observed in the ^1H NMR spectra in the cases of erbium and ytterbium. Although this suggests that at least some of this family of complexes may be kinetically labile, no lanthanide-containing hydrolysis products that may be anticipated from this side reaction were identified in the product mixtures.

Structures of the Complexes in the Solid State

Crystals of representative complexes suitable for X-ray diffraction analysis were grown from CH_2Cl_2/*n*-hexane ($[PrL^{py}]^{3+}$ and $[YbL^{py}]^{3+}$) and MeCN/Et_2O ($[NdL^{py}]^{3+}$,

(9) (a) Wada, A.; Watanabe, B.; Yamanoi, Y.; Nankawa, T.; Namiki, K.; Yamasuki, M.; Murata, M.; Nishihara, H. *Bull. Chem. Soc. Jpn.* **2007**, *80*, 335. (b) Wada, A.; Watanabe, B.; Yamanoi, Y.; Nishihara, H. *Chem. Commun.* **2008**, 1671.

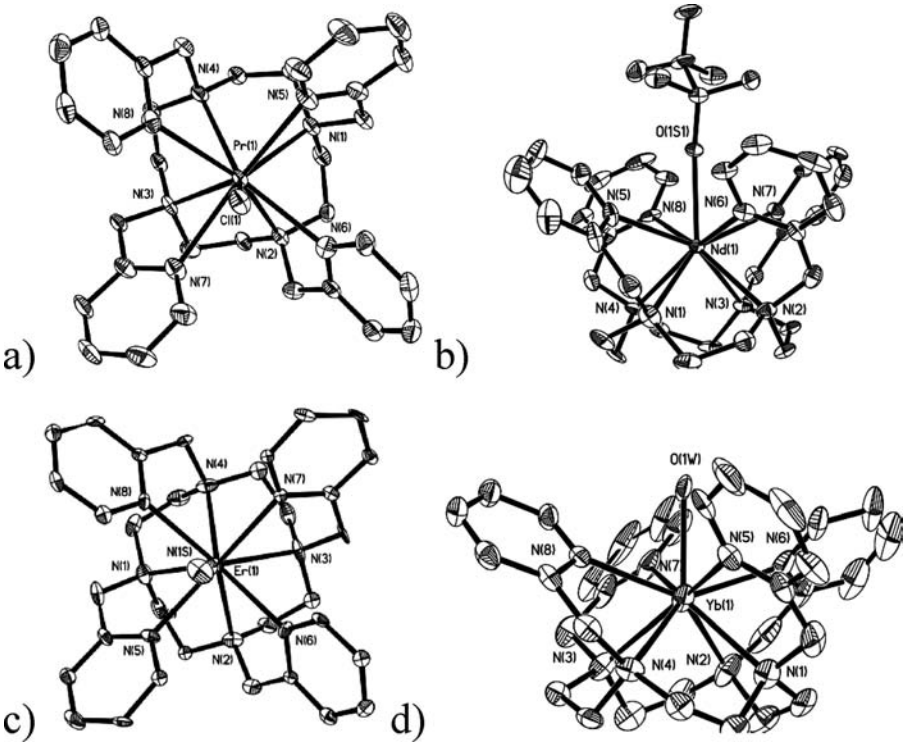

Figure 4. Thermal ellipsoid drawings of (a) $[PrL^{py}(Cl)][OTf]_2$, (b) $[Nd(L^{py})(OTf)][OTf]_2$, (c) $[ErL^{py}(OH_2)][OTf]_3$, and (d) $[YbL^{py}(OH_2)][OTf]_3$, slightly offset view down the C_4 axis (Pr and Er) and the side view (Nd and Yb). 50% ellipsoids, H atoms, lattice counterions, and solvent molecules are omitted for clarity. These can be compared with the structures in ref 9.

$[EuL^{py}]^{3+}$, $[GdL^{py}]^{3+}$, $[TbL^{py}]^{3+}$, and $[ErL^{py}]^{3+}$) despite the high lability of the ytterbium and erbium complexes in solution mentioned above; molecular representations are shown in Figure 4. Unusually for a series of lanthanide complexes, the molecular structures are all 9-coordinate in the solid state. The coordination geometries are approximately monocapped square-antiprismatic, where, in each structure, the four cyclen N atoms [N(1)−N(4)] describe the basal plane and the picolyl N donors [N(5)−N(8)] form the apical plane. The occupancy of the axial or capping position varies according to the 9-coordinate lanthanide ionic radius and the experimental conditions from which the crystals were obtained; the lighter lanthanides (Pr^{3+}, Nd^{3+}, and Eu^{3+}) favor coordination of a counterion, while the heavier metal ions accommodate a solvent molecule, either water (Gd^{3+} and Yb^{3+}) or acetonitrile (Tb^{3+} and Er^{3+}) in the axial position. In the case of the praseodymium complex, a residual chloride anion is ligated to the metal rather than a triflate ion, resulting from use of the sodium chloride adduct of the ligand in the synthesis. Figure 5 shows a stereoplot of the water placement in the hydrated complex $[YL^{py}(OH_2)]^{3+}$ calculated using DFT. The similarity between this structure and the crystal structure shown in Figure 4d is clearly apparent.

Lanthanide complexes of DOTA and its functionalized derivatives have been shown to exist as two enantiomeric pairs of diastereomers arising from two structurally independent elements of chirality associated with the 12-N_4 ring N−C−C−N and pendant arm N−C−C−O torsion angles ($\delta\delta\delta\delta$ or $\lambda\lambda\lambda\lambda$) and the handedness of the pendant arm spatial arrangement (clockwise, Δ, and anticlockwise, Λ).[1] These stereoisomeric forms may interconvert in solution via cyclen ring inversion or pendant arm rotation, and their solution populations are specific for a given lanthanide ion

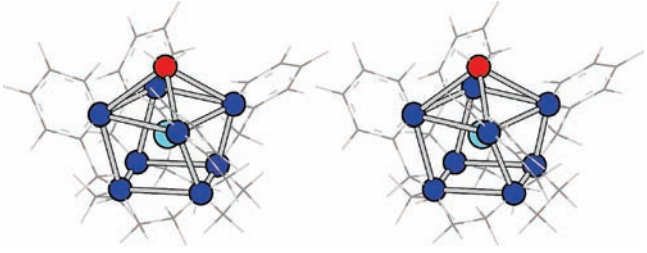

Figure 5. Stereoplot of water placement in $[YL^{py}(OH_2)]^{3+}$ (DFT).

and substituted macrocycle. In the case of the L^{py} complexes, the 8- or 9-coordinate stereoisomers either adopt regular square-antiprismatic coordination geometries or possess a twisted square-antiprismatic structure (rotated about the C_4 axis, approximately halfway between idealized prismatic and antiprismatic geometries).

The solid-state coordination geometry of the lanthanide complexes of L^{py} changes across the series in line with the lanthanide contraction, and there is a clear structural break at gadolinium. The structure types observed, dihedral angles between donor atom planes, and mean $N-C-C-N_{cyclen}$ and $N-C-C-N_{picolyl}$ torsion angles are shown in Table 1, together with comparable data for selected DOTA,[10] DOTAM,[11] and DTMA[12] derivatives. The larger lanthanides crystallize as the monocapped twisted square-antiprismatic

(10) (a) Benetollo, F.; Bombieri, G.; Calabi, L.; Aime, S.; Botta, M. *Inorg. Chem.* **2003**, *42*, 148. (b) Benetollo, F.; Bombieri, G.; Aime, S.; Botta, M. *Acta Crystallogr., Sect. C* **1999**, *55*, 353. (c) Spirlet, M. R.; Rebizant, J.; Desreux, J. F.; Loncin, M.-F. *Inorg. Chem.* **1984**, *23*, 359. (d) Aileen, K. O.; Morrow, J. R.; Lake, C. H.; Churchill, M. R. *Inorg. Chem.* **1994**, *33*, 656. (e) Chang, C. A.; Francesconi, L. C.; Malley, M. F.; Kumar, K.; Gougoutas, J. Z.; Tweedle, M. F.; Lee, D. W.; Wilson, L. J. *Inorg. Chem.* **1993**, *32*, 3501.

Table 1. Structure Types and Dihedral and Torsion Angles for the L^{py} Complexes, with Values for Some DOTA, DOTAM, and DTMA Complexes Shown for Comparison

complex	geometry	dihedral angle (deg)[a]	configuration	ave. cyclen torsion angle (deg)[b]	ave. pendant donor torsion angle (deg)[b]	Ln−axial donor distance (Å)	mean N_{cyclen}−Ln distance (Å)[b]	mean N/ $O_{pendamt}$−Ln distance (Å)[b]	N_4−cyclen centroid−Ln distance (Å)[b]	N_4/O_4 donor centroid−Ln distance (Å)[b]
$[Pr.L^{py}(Cl)]^{2+}$	TSAP′	25	Δ(δδδδ)	+60.1	+29.5	2.7654(11)	2.691(4)	2.668(4)	1.702	0.828
$[Nd.L^{py}(OTf)]^{2+}$	TSAP′	24	Λ(λλλλ)	−58.6	−30.9	2.516(5)	2.666(7)	2.649(7)	1.658	0.854
$[Eu.L^{py}(OTf)]^{2+}$	TSAP′	25	Δ(δδδδ)	+58.3	+31.2	2.507(10)	2.646(15)	2.603(14)	1.647	0.863
$[Gd.L^{py}(OH_2)]^{3+}$	SAP′	36	Λ(δδδδ)	+55.8	−26.9	2.409(15)	2.61(3)	2.57(2)	1.566	0.801
$[Tb.L^{py}(MeCN)]^{3+}$	SAP′	37	Λ(δδδδ)	+60.0	−34.9	2.545(16)	2.623(15)	2.554(15)	1.571	0.829
$[Er.L^{py}(MeCN)]^{3+}$	SAP′	38	Λ(δδδδ)	+58.5	−35.0	2.531(5)	2.591(5)	2.516(5)	1.536	0.860
$[Yb.L^{py}(OH_2)]^{3+}$	SAP′	40	Λ(δδδδ)	+57.6	−32.9	2.398(5)	2.604(7)	2.499(8)	1.565	0.798
$[Ce.DOTA(OH_2)]^{-}$ [10a]	TSAP′	25	Λ(δδδδ)	+58.0	+27.5	2.590	2.738	2.453	1.770	0.758
$[Nd.DOTA(OH_2)]^{-}$ [10a]	SAP′	39	Δ(λλλλ)	−60.1	+23.0	2.508(2)	2.704(2)	2.416(2)	1.676	0.684
$[Eu.DOTA(OH_2)]^{-}$ [10c]	SAP′	39	Λ(δδδδ)	+59.5	−23.1	2.483(3)	2.680	2.394	1.650	0.711
$[Gd.DOTA(OH_2)]^{-}$ [10e]	SAP′	40	Λ(δδδδ)	+59.4	−22.4	2.463	2.663	2.368	1.634	0.720
$[Ho.DOTA(OH_2)]^{-}$ [10b]	SAP′	39	Λ(δδδδ)	+59.2	−22.4	2.443	2.641	2.330	1.608	0.728
$[Pr.DOTAM(OH_2)]^{3+}$ [11a]	TSAP′	23	Δ(δδδδ)	+59.5	+24.4	2.516	2.729	2.443	1.744	0.784
$[Gd.DOTAM(OH_2)]^{3+}$ [11a]	SAP′	37	Δ(λλλλ)	−59.0	+23.7	2.395	2.652	2.380	1.591	0.748
$[Yb.DOTAM(OH_2)]^{3+}$ [11b]	SAP′	40	Λ(δδδδ)	+58.3	−22.5	2.335	2.608	2.301	1.566	0.739
$[Gd.DTMA(OH_2)]^{3+}$ [12b]	SAP′	38	Λ(δδδδ)	+58.7	−29.4	2.461	2.636	2.387	1.591	0.742
$[Dy.DTMA(OH_2)]^{3+}$ [12b]	SAP′	39	Δ(λλλλ)	−58.7	+30.6	2.427(2)	2.636	2.355	1.599	0.754

[a] Error on measurement ±1°. [b] Estimated standard deviation data not available or calculated on some of these numbers.

(TSAP′) diastereoisomer [Δ(δδδδ) and Λ(λλλλ) configurations]. The rotation or twist angle between the cyclen N plane and that of the picolyl N atoms (ϕ) is characteristic of the twisted or inverted square-antiprismatic coordination polyhedron observed in many tetrasubstituted cyclen derivatives, and its value is constant within error (±1°) up to europium.

The smaller lanthanides also crystallize as racemates but as the monocapped square-antiprismatic conformation (SAP′); both λ and δ forms [Λ(δδδδ) and Δ(λλλλ)] are observed in the asymmetric unit cell (Gd^{3+}, Tb^{3+}, and Er^{3+}).[10] In these cases, torsion angles are generally larger than the values measured for the TSAP′ diastereoisomer (Pr−Eu) and are also larger than those found in [Eu.(DOTA)]$^-$, which crystallizes in the SAP′ geometry. In the anomalous case of $[Gd(L^{py})]^{3+}$, however, smaller N−C−C−N torsion angles suggest that the $12N_4$ ring is more strained in this system and the pendant arm layout deviates somewhat from idealized geometry. This is reflected in the dihedral angle between the N_{cyclen} and $N_{picolyl}$ faces, which here increases with increasing nuclear charge, with the ytterbium complex adopting a geometry closest to that of an idealized monocapped square antiprism.

The coordination geometries observed in our system differ from lanthanide complexes of DOTA, where monocapped twisted square-antiprismatic (TSAP′) geometries are observed only in the very early part of the series (Ln = La and Ce). The middle and later parts of the lanthanide series are dominated by the monocapped square antiprism (SAP′). The DOTA series also contains a structural anomaly; [TmDOTA]$^-$ crystallizes as the 8-coordinate TSAP diastereoisomer. The still more compact 8-coordinate unhydrated SAP configuration (ϕ = 41°) is only observed for the group III analogue [ScDOTA]$^-$. Compared to lanthanide DOTA complexes, complexes with L^{py} also show much smaller variations in their dihedral angle for a given coordination environment. The complexes of L^{py} show much greater similarities to neutral primary tetraamide derivatives of DOTA (DOTAM; Figure 1), where the $[PrDOTAM]^{3+}$ complex is isolated as the TSAP′ isomer and the $[Gd^{3+}]$[10b] and $[Yb^{3+}]$[10c] complexes crystallize as the SAP′ isomer (ϕ = 37° and 40°, respectively), though $[EuDOTAM]^{3+}$ is an intermediate case (ϕ = 30°).[13] However, when the amide NH_2 is derivatized further, the steric demands of the ligand change and the SAP′ isomer is consequently observed earlier in the lanthanide series.[12]

The most significant difference between the L^{py} complexes and more conventional N_4O_4 donor sets lies in the position of the lanthanide ions relative to the donor atom planes. Lanthanide ions in all of the solid-state structures of $[LnL^{py}]^{3+}$ lie approximately twice as far from the N_4−cyclen plane as from the N_4−picolyl plane. The average deviation of the metal ions from the N atoms in their respective planes changes according to the coordination isomer; a small variation in Ln−N_4−picolyl distance relative to the Ln−N_4−cyclen distance is also observed across the series. The average values for deviation from the picolyl and cyclen planes for the TSAP′ diastereoisomer are 1.67(5) Å (N_{cyclen}) and 0.85(5) Å ($N_{picolyl}$), respectively. In the SAP′ isomer, these devations are 1.56(7) and 0.82(6) Å, respectively. For comparison, the Ln−N_4−cyclen distances in $[CeDOTA]^-$ and $[PrDOTAM]^{3+}$, which adopt a TSAP′ geometry, are longer at 1.770 and 1.744 Å and the Ln−O_4−acetate/amide distances are significantly shorter, 0.758 and 0.784 Å. The $[NdDOTA]^-$ and $[GdDOTAM]^{3+}$ analogues, which exist in the SAP′ configuration, show a similar trend; crystallographic Ln−N_4−cyclen distances are respectively 1.676 and 1.591 Å, while the Ln−O_4−acetate/amide distances are 0.684 and 0.748 Å. Such discrepancies in these geometric factors between lanthanide complexes of L^{py}

(11) (a) Bombieri, G.; Marchini, N.; Ciattini, S.; Mortillaro, A.; Aime, S. *Inorg. Chim. Acta* **2006**, *359*, 3405. (b) Zhang, S.; Michaudet, L.; Burgess, S.; Sherry, A. D. *Angew. Chem., Int. Ed.* **2002**, *41*, 1919. (c) Thompson, A. L.; Parker, D.; Fulton, D. A.; Howard, J. A. K.; Pandya, S. U.; Puschmann, H.; Senanayake, P. K.; Stenson, P. A.; Badari, A.; Botta, M.; Avedano, S.; Aime, S. *Dalton Trans.* **2006**, 5605. (d) Barge, A.; Botta, M.; Parker, D.; Pushmann, H. *Chem. Commun.* **2003**, 1386.

(12) (a) Aime, S.; Barge, A.; Bruce, J. I.; Botta, M.; Howard, J. A. K.; Maloney, J. M.; Parker, D.; de Sousa, A. S.; Woods, M. *J. Am. Chem. Soc.* **1999**, *121*, 5762. (b) Alderighi, L.; Bianchi, A.; Calabi, L.; Dapporto, P.; Giorgi, C.; Losi, P.; Paleari, L.; Paoli, P.; Rossi, P.; Valtancoli, B.; Virtuani, M. *Eur. J. Inorg. Chem.* **1998**, 1581. (c) Dickins, R. S.; Parker, D.; Bruce, J. I.; Tozer, D. J. *Dalton Trans.* **2003**, 1264. (d) Dickins, R. S.; Howard, J. A. K.; Maupin, C. L.; Moloney, J. M.; Parker, D.; Riehl, J. P.; Siligardi, G.; Williams, J. A. G. *Chem.—Eur. J.* **1999**, *5*, 1095.

(13) Amin, S.; Voss, D. A.; Horrocks, W. de W.; Lake, C. H.; Churchill, M. R.; Morrow, J. R. *Inorg. Chem.* **1995**, *34*, 3294.

Table 2. Photophysical Properties of the Neodymium, Praseodymium, Samarium, Europium, and Terbium Complexes

complex	λ_{ex}/nm	λ_{em}/nm	$\tau_{H_2O}/\mu s$	$\tau_{D_2O}/\mu s$	q_{H_2O}	$\tau_{CH_3OH}/\mu s$	$\tau_{CD_3OD}/\mu s$	q_{CH_3OH}
$[NdL^{py}]^{3+}$	337	1055	0.10 (62%), 0.23 (38%)	0.19 (53%), 0.36 (47%)	0.3, 0	0.12 (52%), 0.33 (48%)	0.24 (23%), 0.43 (77%)	0.1, 0
$[PrL^{py}]^{3+}$	337	1030	weak	0.06 (65%), 0.12 (35%)	*a*	weak	0.15 (60%), 0.21 (40%)	*a*
$[SmL^{py}]^{3+}$	405	650	12.5	20.0		27.7	30.6	
$[EuL^{py}]^{3+}$	260	617	720	1300	0.4	680	790	0.2
$[TbL^{py}]^{3+}$	260	545	2060	2540	0.2	2210	2570	0.3

[a] No reliable parameters exist for determining *q* values for praseodymium. All others were determined using established parameters,[15] though it should be stressed that the parameters for neodymium complexes are unreliable as a consequence of facile C−H quenching by ligand oscillators and the consequent dependence of the apparent value of *q* upon the structure of the ligand bound to neodymium.

and those of DOTA and DOTAM indicate that the metal ions in the picolyl complexes are displaced less toward the plane defined by the pendant arm donors, as a consequence of the use of N as a donor atom rather than O.

This difference in donor set anisotropy in complexes of L^{py} with respect to those of DOTA is not, however, mirrored in the solid-state bond distances (Table 1); the mean $Ln-N_{cyclen}$ distances mirror those in the $[Ln.DOTA]^-$ series, while the N−picolyl distances are comparable with those in complexes with tris(2-pyridylmethyl)amine.[14] Similarly, the $Ln-H_2O$ distances in $[GdL^{py}]^{3+}$ and $[YbL^{py}]^{3+}$ are within error of one another and comparable to those for SAP′ isomers of $[LnDOTA]^-$ and $[LnDOTAM]^{3+}$ complexes.

Structure in Solution

The structure of the complexes in solution was probed by luminescence and NMR spectroscopy. All of the complexes with the exception of $[GdL^{py}]^{3+}$ are luminescent in solution, with emission spectra spanning the visible and near-IR regions of the spectrum, though detailed analysis of the photophysical properties of the erbium and ytterbium complexes was not carried out owing to their lability in solution. Luminescence lifetime measurements were carried out in both aqueous and methanolic solutions. It can be seen from Table 2 that double-exponential fitting is required for the neodymium and praseodymium complexes, while the europium and terbium complexes exhibit single-exponential decay kinetics, with no significant improvement in the fit when a second exponential component is added. The lifetimes obtained in normal and deuterated solvents were used to calculate the inner-sphere solvation numbers for the neodymium, europium, and terbium complexes from the equation

$$q = A(k_H - k_D - B) \quad \text{and} \quad q = A(k_H - k_D) - B(\text{Nd})$$

where k_H and k_D are the observed rate constants for the luminescence in H_2O and D_2O and *A* and *B* are established constants for each lanthanide.[15] The results are summarized in Table 2.

The kinetic stability of the complexes in solution was assessed by carrying out a competitive binding study with diethylenetriaminepentaacetic acid (DTPA) while observing the luminescence lifetime and ^1H NMR spectrum. Upon the addition of 1 equiv of DTPA to an aqueous solution of $[EuL^{py}]^{3+}$, the luminescent lifetimes in both H_2O and D_2O are immediately reduced from the values reported in Table 2 to 0.547 and 1.00 ms, respectively; the resultant inner-sphere hydration number increases to 0.7. $[EuDTPA]^{2-}$ possesses a calculated inner-sphere hydration number of 1.1.[16] A similar competitive binding experiment was studied by NMR: the ^1H NMR spectral resonances of $[EuL^{py}]^{3+}$ change to closely resemble the known complex $[EuDTPA]^{2-}$. Following the changes observed immediately after the addition of DTPA, both ^1H NMR spectra and luminescence lifetimes remained unchanged after 10 min and again after 24 h. These data suggest that the kinetic stability of $[EuL^{py}]^{3+}$ is low and that competitive binding of $[EuL^{py}]^{3+}$ with DTPA principally affords $[EuDTPA]^{2-}$ and a second, minor Eu^{3+}-containing species, not identified.

It remains to explain the difference in the observed behavior between europium and terbium and the other lanthanides. Europium and terbium both have very long luminescence lifetimes when compared to the other lanthanides, and any species in rapid exchange relative to this millisecond-order time scale will appear as a single, averaged, entity. By contrast, the other lanthanides have much shorter luminescence lifetimes, on which such averaging is less likely. On this basis, we postulated that an equilibrium exists between two species, one of which has a single bound inner-sphere solvent molecule, while the other has none. This hypothesis is supported by the calculated *q* values, which show intermediate values for europium and terbium and which have one component corresponding to a $q = 0$ complex for the systems in which double-exponential fitting is used. However, the nature of the luminescence processes preclude detailed analysis of the composition of the mixtures because the quantum yields for the $q = 0$ and 1 complexes will be very different owing to increased nonradiative quenching of the emissive state by bound solvent oscillators in the latter case.

The structure of the complexes was studied further by ^1H NMR spectroscopy. All of the complexes exhibit shifted and broadened NMR spectra at 500 MHz in D_2O at ambient temperature (Figure 6), consistent with the presence of a bound paramagnetic lanthanide ion, although the range of chemical shifts is substantially less than that observed in the spectra of the corresponding DOTA complexes.[8a]

The ^1H NMR spectra of most L^{py} complexes show more than one geometric isomer (~2% minor isomers for Pr and Nd; ~15% for Eu and Tb; ~40% for Dy). Interconversion between the major and minor isomers was investigated further for the europium complex, which has a favorable ratio of pseudo contact shift (PCS) to line broadening. At 298 K, the complex shows predominantly two isomers (accounting for >99% of the signal) in a molar ratio of 85:15. COSY, EXSY, and HSQC spectroscopy yielded complete signal assignments in both ^1H and $^{13}C\{^1H\}$ spectra (Figure 7) and demonstrated

(14) Natrajan, L. S.; Pecaut, J.; Mazzanti, M.; LeBrun, C. *Inorg. Chem.* **2005**, *44*, 4756.
(15) Beeby, A.; Clarkson, I. M.; Dickins, R. S.; Faulkner, S.; Parker, D.; Royle, L.; de Sousa, A. S.; Williams, J. A. G.; Woods, M. *J. Chem. Soc., Perkin Trans. 2* **1999**, 493.
(16) Supkowski, R. M.; Horrocks, W. de W. *Inorg. Chim. Acta* **2002**, *340*, 44.

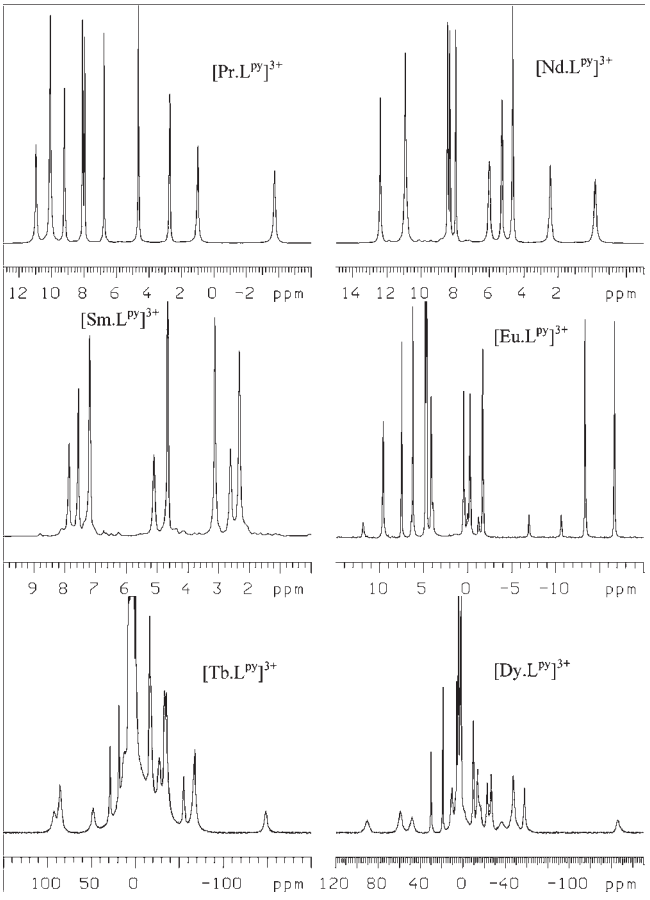

Figure 6. ^{1}H NMR spectra (500 MHz, D_2O) of six paramagnetic $[LnL^{py}]^{3+}$ complexes.

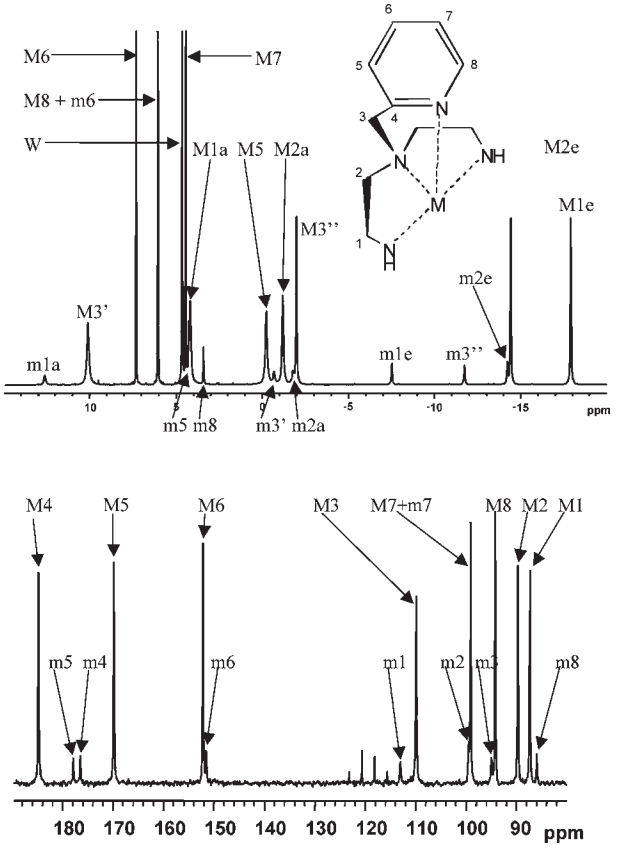

Figure 7. Annotated ^{1}H (top) and $^{13}C\{^1H\}$ (bottom) NMR spectra for $[EuL^{py}][OTf]_3$ in D_2O at 500 and 125 MHz, respectively. Numbers used in the assignments refer to the structure on the ^{1}H NMR spectrum, where "M" denotes the major isomer and "m" the minor. The spectra were recorded at 273 K to afford slightly improved resolution between the major and minor isomers.

that interconversion between the two forms, although slow, is detectable on the NMR time scale and involves exchange between a high-frequency peak in the ^{1}H NMR spectrum (+12.5 ppm) with the lowest frequency (−16.8 ppm), which is in marked contrast to the behavior observed in the EXSY spectrum of the analogous DOTA complex.

DFT was used to calculate the energies for the various forms. All possible isomeric forms exist in thermodynamic equilibrium in solution (relative populations being specific to each lanthanide) and interconvert via cyclen ring inversion or pendant arm rotation.[1] Yttrium(III) was used for DFT calculations to avoid computational issues associated with open f shells and relativistic core electrons of lanthanides.

Figure 8 shows a DFT scan through the cyclen ring isomerization path for the yttrium analogue of the complexes in question. A synchronous four-joint inversion (i.e., directly from A to B) appears to be impossible because the associated activation energy is in excess of 200 kJ/mol; the isomerization path is instead a sequence of single-joint inversions.

The saddle points associated with each of the elementary reactions in Figure 8 are shown in Figure 9. All four saddles correspond to one of the N−C−C−N dihedral angles twisting into an eclipsed conformation. The associated activation energies (Table 3) are in the region of 50 kJ/mol.

Experimentally, only the low-energy $\delta\delta\delta\delta$ (Minimum A) and $\lambda\lambda\lambda\lambda$ (Minimum B) conformations are normally visible.[1b] Because of the multistage nature of the isomerization process, any experimentally measured activation energies would be effective over the four stages shown in Figure 8.

The effective activation energy of the isomerization between $\delta\delta\delta\delta$ and $\lambda\lambda\lambda\lambda$ forms was measured by selective inversion of ^{1}H NMR signals in the temperature range of −4.6 to +22.6 °C (measured using methanol chemical shifts). The peak of the major form at −16.8 ppm was inverted and the effect on its exchange partner in the minor form at +12.5 ppm observed as a function of the mixing time. The results were analyzed using the *CIFIT-2* program,[18] taking into account the independently measured T_1 values for the two peaks, yielding an effective Arrhenius activation energy of 79 ± 3 kJ/mol, in good agreement with the DFT results. A global multiline asymmetric chemical exchange fit to experimental data (Figure 10) performed for selected ^{13}C NMR signals from the pyridyl rings in the −0.2 to +53.8 °C temperature range resulted in $\Delta H^{\ddagger}_f$ = 76.4 kJ/mol, $\Delta S^{\ddagger}_f$ = 29.9 J/mol·K, $\Delta H^{\ddagger}_b$ = 85.6 kJ/mol, and $\Delta S^{\ddagger}_b$ = 47.0 J/mol·K for the forward and backward processes, respectively.

Attempts to assign the observed spectra by calculation of the PCSs based on the DFT geometries calculated for the two isomeric structures were unsuccessful, presumably because of the failure of the point dipole approximation in this case. It has been shown that the point dipole approximation works reasonably well in the cases of DOTA derivatives where the ligand donor set consists of four N atoms and

(17) (a) Peng, C.; Schlegel, H. B. *Isr. J. Chem.* **1993**, *33*, 449. (b) Peng, C.; Ayala, P. Y.; Schlegel, H. B.; Frisch, M. J. *J. Comput. Chem.* **1996**, *17*, 49.
(18) Bain, A.; Fletcher, D. A. *Mol. Phys.* **1998**, *95*, 1091.

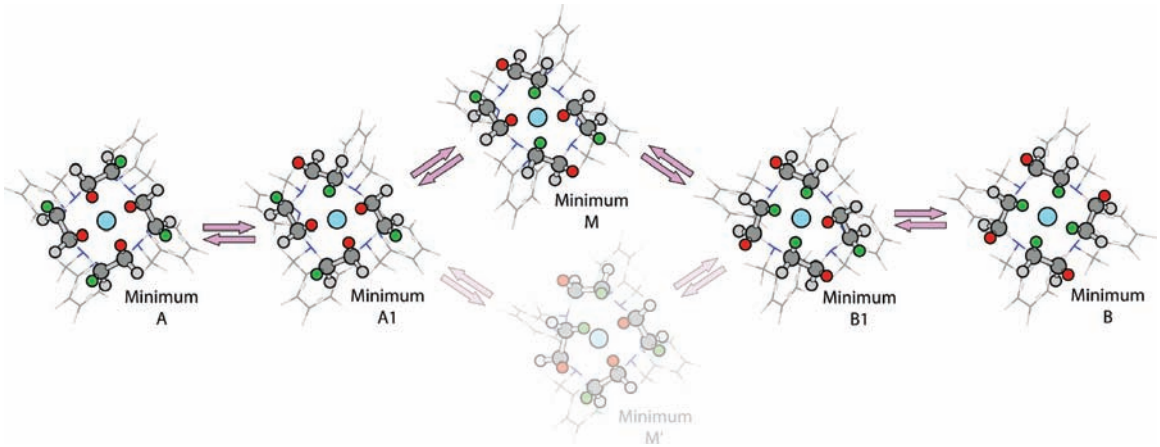

Figure 8. Quadratic synchronous transit[17] trace through the isomerization path of $[Y(L^{py})]^{3+}$ (only minima are shown; see Figure 9 for saddle points). The isomerization process is a sequence of single-joint inversions (energies are given in Table 3). The grayed-out structure (Minimum M') is over 10 kJ/mol higher in energy than its alternative (Minimum M).

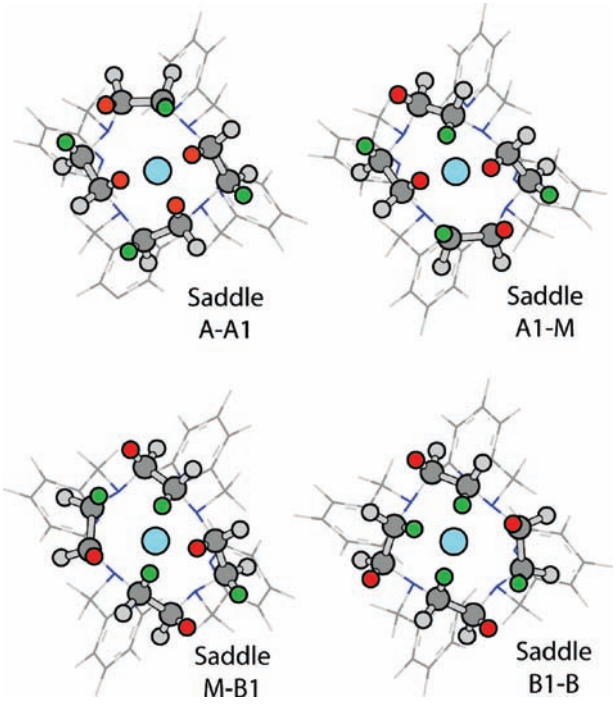

Figure 9. Saddle points associated with the reaction path shown in Figure 1, obtained using the QST2 method. The corresponding energies are given in Table 3. The structures (including Hessians) are available from the Supporting Information.

four O atoms[8,19] so that the crystal-field term in the Bleaney equation[20] is presumably dominated by the dipole along the axis of symmetry of the ligand. In the present case, the ligand donor set consists of eight N atoms, which means that the dipole along the axis of symmetry of the ligand is much smaller (approximately zero), leading to the breakdown of the point dipole approximation. Significantly, it is also observed that the point dipole approximation fails in the case of paramagnetic lanthanide complexes of the Lehn cryptand,

Table 3. DFT Energies of the Minimum and Saddle Points Shown in Figures 8 and 9

	energy (kJ/mol)		
minimum/saddle	vacuum[a]	vacuum with coordinated water[a]	PCM water + coordinated water[b]
A	0.0	0.0	0.0
A−A1	60.8	56.8	55.9
A1	32.0	24.6	24.0
A1−M	64.4	54.1	54.8
A1−M′	70.4	62.3	60.0
M	36.6	20.8	21.6
M′	41.1	37.9	33.4
M−B1	81.0	59.9	58.8
M′−B1	73.4	69.5	65.7
B1	41.0	20.6	17.1
B1−B	78.0	61.4	58.8
B	24.0	6.1	2.0

[a] DFT B3LYP cc-pVDZ (Stuttgart RSC 1997 ECP on Y). [b] DFT B3LYP cc-pVTZ (Stuttgart RSC 1997 ECP on Y).

which is another highly symmetric eight-N donor set, though of a different geometry.[21] The importance of the axial dipole in determining the spectroscopic properties of related ligands has also been demonstrated experimentally.[12c,22]

Summary and Conclusions

A series of lanthanide(III) complexes of tetrapicolyl-substituted cyclen (L^{py}) have been prepared. The solid-state structures are all 9-coordinate and show a variation in the coordination geometry from TSAP′ to SAP′ across the series.

In solution, time-resolved luminescence studies show the existence of two species on the nanosecond time scale and averaged values on the millisecond time scale, suggesting the slow exchange of inner- and outer-sphere water. Dynamic NMR studies on the europium complex show that the interconversion of the two isomers is slow on the NMR time scale and occurs by arm rotation, with an apparent free-energy barrier to isomerism of 76 kJ/mol. DFT calculations on the yttrium analogue are in broad agreement with this

(19) (a) Desreux, J. F. *Inorg. Chem.* **1980**, *19*, 1319. (b) Hoeft, S.; Roth, K. *Chem. Ber.* **1993**, *126*, 869. (c) Forsberg, J. H.; Delaney, R. M.; Zhao, Q.; Harakas, G.; Chandran, R. *Inorg. Chem.* **1995**, *34*, 3705.
(20) Bleaney, B. *J. Magn. Reson.* **1972**, *8*, 91.
(21) Faulkner, S.; Beeby, A.; Carrie, M.-C.; Dadabhoy, A.; Kenwright, A. M.; Sammes, P. G. *Inorg. Chem. Commun.* **2001**, *4*, 187.
(22) Di Bari, L.; Pintacuda, G.; Salvadori, P.; Dickins, R. S.; Parker, D. *J. Am. Chem. Soc.* **2000**, *122*, 9257.

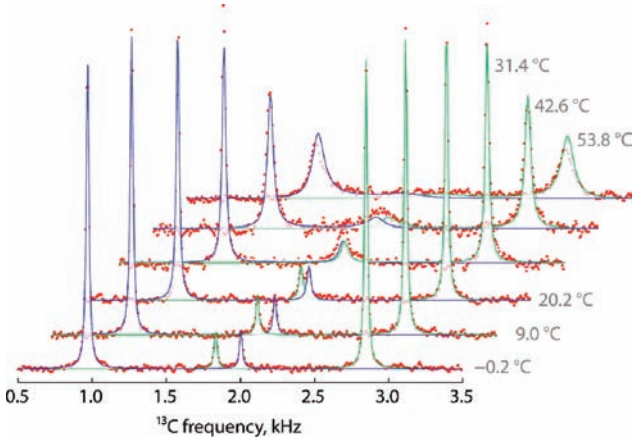

Figure 10. Global chemical exchange fits, using Bloch equations, of the signals belonging to two pairs of exchanging pyridyl signals in the $^{13}C\{^1H\}$ NMR spectrum of $[EuL^{py}][OTf]_3$ in D_2O.

overall free-energy barrier and, importantly, show that conformational exchange proceeds via a series of arm rotations rather than a concerted pathway in this system.

It is also worth noting that this ligand system has a high degree of ligand symmetry (eight N donor atoms), which results in a much reduced range of PCSs compared with less symmetric systems such as the DOTA analogues (four O and four N donor atoms).

Experimental Section

DFT Calculations. The DFT calculations were performed for yttrium(III) complexes (which are known to have strong structural similarities to lanthanide complexes,[1] being at the same time more straightforward theoretically than open-shell lanthanides) using the *Gaussian03* package.[23] Molecular geometries were optimized in vacuo using a spin-restricted B3LYP exchange-correlation functional with a compound basis set (cc-pVDZ for CHNO and Stuttgart RSC 1997 ECP[24] for yttrium). Transition states were located using the QST2 method.[17] Hessians were computed and intrinsic reaction coordinates traced in both directions to ensure that the transition states are first-order saddles corresponding to the process under consideration. Energies were computed for converged saddles and stationary points with the cc-pVTZ basis set on CHNO (the yttrium basis set was kept unchanged) in PCM water.

NMR Measurements and Assignment. All NMR spectra of diamagnetic compounds were recorded on a Bruker Avance 400 spectrometer, with operating frequencies 400 MHz (^{1}H) and 100 MHz (^{13}C) and the variable-temperature unit set at 300 K, unless otherwise stated. Chemical shifts are reported in parts per million relative to tetramethylsilane ($SiMe_4$) and referenced to the residual proton resonances in deuterated solvents. NMR spectra of paramagnetic compounds were recorded primarily on a Varian Inova 500, with operating frequencies 500 MHz (^{1}H) and 125 MHz (^{13}C) at 295 K. Additional ^{1}H NMR spectra were recorded at ambient temperature (around 295 K) using Varian Mercury 200, Varian Mercury 400, and Varian VNMRS 700 spectrometers. An accurate sample temperature was measured by substitution using methanol at temperatures below 299 K and ethylene glycol at higher temperatures.

For the $[EuL^{py}]^{3+}$ complex, initial ^{1}H assignments were made using COSY spectra to establish methylene pairs and identify the cyclen ring in the major isomer. ^{1}H EXSY spectra with a mixing time of 100 ms were used to establish the correspondences between the major and minor isomers. ^{13}C assignments for the major isomer and the majority of peaks in the minor isomer were made using HSQC (confirming methylene assignments from COSY). Dynamic processes were studied over a range of temperatures using ^{1}H selective inversion experiments to invert the most shifted peak in the spectrum of the major isomer and observe the effect on the corresponding peak in the spectrum of the minor isomer as a function of the mixing time. They were also studied by observation of the line-shape changes in the ^{13}C NMR spectrum as a function of the temperature. ^{13}C assignments for the remaining minor isomer peaks were made by observation of coalescence with assigned major isomer peaks at high temperatures. ^{1}H T_1 values were measured by inversion−recovery and were used in analysis of the selective inversion experiments using the *CIFIT-2* program.[18] Relevant spectra are included in the Supporting Information.

Crystallography. Data Collection and Processing. Data for compounds L^{py}, $[L^{py}H_2][OTf]_2$, $[PrL^{py}(Cl)][OTf]_2$, $[NdL^{py}(OTf)][OTf]_2$, $[EuL^{py}(OTf)][OTf]_2$, $[TbL^{py}(MeCN)][OTf]_3$, $[ErL^{py}(MeCN)][OTf]_3$, and $[YbL^{py}(OH_2)][OTf]_3$ were collected at 100 K with an Oxford Diffraction XCalibur2 diffractometer equipped with an Oxford Cryosystems low-temperature device[25] using Mo Kα radiation and ω scans. Data were corrected for Lorenz and polarization factors and absorption corrections applied to all data. Data for compound $[GdL^{py}(OH_2)][OTf]_3$ were collected on a Nonius κ-CCD four-circle diffractometer using graphite-monochromated Mo Kα radiation at 150 K. Absorption corrections were applied by the multiscan method using the *SORTAV* program.[26]

Structure Analysis and Refinement. All structures were solved by direct methods using *SHELXS-97*[27] or *SIR-92*[28] running in *WIN-GX*.[29] All structures were completed by iterative cycles of ΔF syntheses and a full-matrix least-squares refinement. In compounds L^{py}, $[L^{py}H_2][OTf]_2$, $[PrL^{py}(Cl)][OTf]_2$, $[NdL^{py}(OTf)][OTf]_2$, and $[YbL^{py}(OH_2)][OTf]_3$, all non-H atoms were refined anisotropically, except the disordered solvent molecules and disordered counterions (CH_2Cl_2 and $CF_3SO_3^-$ in $[PrL^{py}(Cl)][OTf]_2$ and $[YbL^{py}(OH_2)][OTf]_3$). In compounds $[EuL^{py}(OTf)][OTf]_2$, $[GdL^{py}(OH_2)][OTf]_3$, $[TbL^{py}(MeCN)][OTf]_3$, and $[ErL^{py}(MeCN)][OTf]_3$, several C, N, and O atoms belonging to lattice counterions were restrained as approximately isotropic to prevent them from going nonpositive definite. All other non-H atoms were refined anisotropically. In all structures, difference Fourier syntheses were employed in positioning idealized H atoms, which were allowed to ride on their parent C or N atoms. All refinements were against F^2 and used *SHEL-XL-97*.[30]

(23) Frisch, M. J.; Trucks, G. W.; Schlegel, H. B.; Scuseria, G. E.; Robb, M. A.; Cheeseman, J. R.; Montgomery, J. A.; Vreven, T.; Kudin, K. N.; Burant, J. C.; Millam, J. M.; Iyengar, S. S.; Tomasi, J.; Barone, V.; Mennucci, B.; Cossi, M.; Scalmani, G.; Rega, N.; Petersson, G. A.; Nakatsuji, H.; Hada, M.; Ehara, M.; Toyota, K.; Fukuda, R.; Hasegawa, J.; Ishida, M.; Nakajima, T.; Honda, Y.; Kitao, O.; Nakai, H.; Klene, M.; Li, X.; Knox, J. E.; Hratchian, H. P.; Cross, J. B.; Bakken, V.; Adamo, C.; Jaramillo, J.; Gomperts, R.; Stratmann, R. E.; Yazyev, O.; Austin, A. J.; Cammi, R.; Pomelli, C.; Ochterski, J. W.; Ayala, P. Y.; Morokuma, K.; Voth, G. A.; Salvador, P.; Dannenberg, J. J.; Zakrzewski, V. G.; Dapprich, S. A.; Daniels, D.; Strain, M. C.; Farkas, O.; Malick, D. K.; Rabuck, A. D.; Raghavachari, K.; Foresman, J. B.; Ortiz, J. V.; Cui, Q.; Baboul, A. G.; Clifford, S.; Cioslowski, J.; Stefanov, B. B.; Liu, G.; Liashenko, A.; Piskorz, P.; Komaromi, I.; Martin, R. L.; Fox, D. J.; Keith, T.; Al-Laham, M. A.; Peng, C. Y.; Nanayakkara, A.; Challacombe, M.; Gill, P. M. W.; Johnson, B.; Chen, W.; Wong, M. W.; Gonzalez, C.; Pople, J. A. *Gaussian 03*, revision C.02; Gaussian, Inc.: Wallingford, CT, 2004.

(24) Stuttgart RSC **1997** ECP.

(25) Cosier, J.; Glazer, A. M. *J. Appl. Crystallogr.* **1986**, *19*, 105.

(26) Blessing, R. H. *Acta Crystallogr.* **1997**, *30*, 563.

(27) Sheldrick, G. M. *SHELX-97*; University of Göttingen: Göttingen, Germany, 1998.

(28) Altomare, A.; Cascarano, G.; Giacovazzo, C.; Guagliardi, A.; Burla, M. C.; Polidori, G.; Camalli, M. *J. Appl. Crystallogr.* **1994**, *27*, 435.

(29) WIN-GX package: Farrugia, L. J. *J. Appl. Crystallogr.*, **1999**, *32*, 837.

(30) *SHELXL-PC Package*; Bruker Analytical X-ray Systems: Madison, WI, 1998.

Luminescence Measurements. Steady-state and time-resolved luminescence properties of the terbium and europium complexes were determined using a PerkinElmer LS55 fluorimeter operating in phosphorescence mode. Steady-state spectra of samarium-containing complexes were also recorded on a PerkinElmer LS55 fluorimeter in phosphorescence mode with an applied delay time of 0.01 ms. Time-resolved luminescence measurements on the samarium complexes were obtained using an Edinburgh Instruments mini-Tau system by time-correlated single photon counting. Lifetimes were obtained by the tail fit on the data obtained and the quality of fit judged by minimization of reduced χ^2 and residuals squared. In the case of the praseodymium, ytterbium, and neodymium complexes, the sample was excited using a pulsed nitrogen laser (337 nm) operating at 10 Hz. Light emitted at right angles to the excitation beam was focused onto the slits of a monochromator, which was used to select the appropriate wavelength. The growth and decay of the luminescence at selected wavelengths was detected using a germanium photodiode (Edinburgh Instruments, EI-P) and recorded using a digital oscilloscope (Tektronix TDS220) before being transferred to a PC for analysis. Luminescence lifetimes were obtained by iterative reconvolution of the detector response (obtained by using a scatterer) with exponential components for growth and decay of the metal-centered luminescence, using a spreadsheet running in Microsoft Excel. The details of this approach have been discussed elsewhere.[31] Unless otherwise stated, fitting to a double-exponential decay yielded no improvement in the fit as judged by minimization of residuals squared and reduced χ^2.

General Methods. Cyclen was purchased from Strem Chemicals, while other reagents, solvents, and starting materials were obtained from Aldrich Chemical Co. All chemicals were used as supplied.

MS spectra were obtained using a positive electrospray in acetonitrile or methanol solutions on a Micromass Platform II spectrometer or by MALDI using methanol solutions with an ALPHA matrix on a Micromass TOF Spec 2E spectrometer.

Elemental analyses were performed using a Carlo ERBA Instruments CHNS-O EA1108 elemental analyzer (C, H, N, and S analysis) and a Fisons Horizon Elemental Analysis ICP-OED spectrometer for metals and halogens.

Absorption spectra were recorded in H_2O on a T60U spectrometer (PG Instruments Ltd.) using fused silica cells with a path length of 1 cm.

Assignments for NMR spectra are given using the numbering scheme shown in Figure 7.

Preparation of 1,4,7,10-Tetrakis(2-pyridylmethyl)-1,4,7,10-tetraazacyclododecane, L^{py}. Under dinitrogen, cyclen (0.659 g, 3.82 mmol) was dissolved in 15 mL of MeCN and 20 mol equiv of Cs_2CO_3 (24.93 g, 76.5 mmol) was added as a solid to form a suspension. A total of 4 mol equiv of 2-picolylchloride hydrochloride in MeCN (2.51 g, 15.3 mmol, 15 mL) was then added dropwise to the cyclen solution, causing a color change from clear to pink and finally to light brown. The reaction mixture was subsequently heated to reflux temperature under nitrogen for 24 h, after which the solution was filtered to remove the inorganic salts, and all volatiles were removed under reduced pressure.

The crude powder was extracted into hot MeCN (100 mL), filtered, and cooled slowly to 4 °C overnight. The resultant crystals were collected by filtration, washed with minimal volumes of MeCN, and dried under vacuum suction to yield analytically pure L^{py}. Further reduction of the supernatant to 5 mL and cooling to −18 °C afforded a second and third crop of crystals to give a total yield of 87% (1.78 g).

(31) Beeby, A.; Faulkner, S. *Chem. Phys. Lett.* **1997**, *266*, 116.

NMR ($CDCl_3$, 298 K): δ_H 8.46 (dd, 4H, $^3J_{HH}$ = 4.9 Hz, $^4J_{HH}$ = 1.7 Hz, H_8), 7.61 (d, 4H, $^3J_{HH}$ = 7.7 Hz, H_5), 7.41 (td, 4H, $^3J_{HH}$ = 7.7 Hz, $^4J_{HH}$ = 1.7 Hz, H_6), 7.07 (dd, 4H, $^3J_{HH}$ = 7.7 and 4.9 Hz, H_7), 3.62 (s, 8H, H_3), 2.76 (s, 16H, H_1, H_2); δ_C 160.1 (q-*C*, C_4), 148.3 (*C*H, C_8), 136.5 (*C*H, C_6), 123.0 (*C*H, C_5), 121.7 (*C*H, C_7), 61.6 (CH_2, C_3), 53.4 (CH_2, C_1, C_2). ES^+-MS: 537 $\{M - H\}^+$ (100%), 559 $\{M - Na\}^+$ (53%). UV−vis [MeOH; λ_{max} (ε (M^{-1} cm^{-1}))]: 256 (sh, 9360), 261 (9770), 268 (sh, 7270). Anal. Calcd for $C_{32}H_{40}N_8$: C, 71.6; H, 7.5; N, 20.9. Found: C, 71.4; H, 7.5; N, 20.8.

Preparation of 1,4,7,10-Tetrakis(2-pyridylmethyl)-1,4,7,10-tetraazacyclododecane Sodium Chloride, $[L^{py}Na]Cl$. The first part of the preparation was identical with that described previously for L^{py}, except that 76.5 mmol of NaCl were used in place of 76.5 mmol of Cs_2CO_3.

The crude powder was recrystallized from dichloromethane/hexane (1:3) to afford the NaCl salt of L^{py} as a light-brown microcrystalline solid in 48% yield (0.98 g).

NMR ($CDCl_3$, 298 K): δ_H 7.62 (td, 4H, $^3J_{HH}$ = 7.7 Hz, $^4J_{HH}$ = 1.7 Hz, H_6), 7.41 (d, 4H, $^3J_{HH}$ = 4.9 Hz, H_8), 7.12 (d, 4H, $^3J_{HH}$ = 7.7 Hz, H_5), 6.97 (dd, 4H, $^3J_{HH}$ = 7.7 and 4.9 Hz, H_7), 4.30−1.40 (br, 24H, H_1, H_2, H_3); δ_C 158.5 (q-C, C_4), 148.8 (*C*H, C_8), 136.9 (*C*H, C_6), 123.8 (*C*H, C_5), 122.4 (*C*H, C_7), 59.1, 53.5, 47.1 (CH_2, C_1, C_2, C_3).

ES^+-MS: 537 $\{M - H\}^+$ (12%), 559 $\{M - Na\}^+$ (100%). UV−vis [MeOH; λ_{max} (ε (M^{-1} cm^{-1}))]: 257 (sh, 9850), 262 (10 130), 269 (sh, 7030). Anal. Calcd for $C_{32}H_{40}N_8 \cdot NaCl \cdot 1.5H_2O \cdot CH_2Cl_2$: C, 56.1; H, 6.4; N, 15.9; Na, 3.3; Cl, 15.0. Found: C, 56.1; H, 6.4; N, 16.1; Na, 2.9; Cl, 14.80.

Analytical Data for Diprotonated L^{py}, $[H_2L^{py}][OTf]_2$. NMR (D_2O, 298 K): δ_H 8.22 (d, 4H, $^3J_{HH}$ = 4.8 Hz, H_8), 7.62 (t, 4H, $^3J_{HH}$ = 7.2 Hz, H_6), 7.48 (d, 4H, $^3J_{HH}$ = 7.2 Hz, H_5), 7.26 (dd, 4H, $^3J_{HH}$ = 7.2 and 4.8 Hz, H_7), 4.13 (s, 8H, H_3), 3.37 (s, 16H, H_1, H_2); δ_C 148.7 (*C*H, C_8), 138.2 (*C*H, C_6), 124.3 (*C*H, C_5), 124.2 (*C*H, C_7), 124.0 (q-*C*, C_4), 57.6 (CH_2, C_3), 49.3 (CH_2, C_1, C_2). ES^+-MS: 559 $\{M - 2OTf + Na\}^+$ (100%), 537 $\{M - 2OTf + H\}^+$ (7%). UV−vis (H_2O; λ_{max}): 254 (sh), 259, 266 (sh).

Preparation of Lanthanide Complexes of L^{py}. Preparation of 1,4,7,10-Tetrakis(2-pyridylmethyl)-1,4,7,10-tetraazacyclododecane Lanthanide Tris(trifluoromethanesulfonate), $[LnL^{py}][OTf]_3$. $[LaL^{py}][OTf]_3$. A solution of L^{py} in methanol (100 mg, 0.186 mmol, 3 mL) was added dropwise to a methanolic solution of $La(OTf)_3$ (109 mg, 0.186 mmol, 2 mL) and the resulting solution was warmed gently to 40 °C. After 24 h, all volatiles were removed under reduced pressure and the crude solid was dissolved in 3 mL of MeCN; 10 mL of diethyl ether was then layered onto this solution. After diffusion was complete (1 week), the precipitated crystalline solid was isolated by filtration, washed with 3 aliquots of diethyl ether (15 mL), and dried under vacuum suction to afford the title compound as a colorless solid (136 mg, 63% yield).

NMR (H_2O, 298 K): δ_H 8.02 (td, 4H, $^3J_{HH}$ = 7.6 Hz, $^4J_{HH}$ = 1.2 Hz, H_6), 7.67 (d, 4H, $^3J_{HH}$ = 4.8 Hz, H_8), 7.56 (d, 4H, $^3J_{HH}$ = 7.6 Hz, H_5), 7.43 (dd, 4H, $^3J_{HH}$ = 7.5 and 4.8 Hz, H_7), 4.38 (d, 4H, $^2J_{HH}$ = 16.4 Hz, H_3), 3.97 (t, 4H, $^2J_{HH}$ = 13.2 Hz, H_{ax} ring), 3.83 (d, 4H, $^2J_{HH}$ = 16.4 Hz, $H_{3'}$), 3.28 (t, 4H, $^2J_{HH}$ = 13.2 Hz, H_{ax} ring), 2.70 (t, 8H, $^2J_{HH}$ = 12.8 Hz, H_{eq} ring).

MALDI-MS (α/MeOH): 1013 $\{M - OTf + K + H\}^+$ (48%), 1052 $\{M - OTf + 2K\}^+$ (12%). UV−vis [H_2O; λ_{max} (ε (M^{-1} cm^{-1}))]: 261 (sh, 11 600), 267 (12 650), 273 (sh, 8350). Anal. Calcd for $C_{35}H_{40}N_8O_9S_3F_9La \cdot 2H_2O$: C, 36.3; H, 3.8; N, 9.7; S, 8.3; La, 12.0. Found: C, 36.6; H, 3.7; N, 9.7; S, 7.7; La, 11.9.

Complexes of other lanthanides were prepared by the same method. Characterization data are provided in the Supporting Information.

Acknowledgment. The authors thank Claudio Luchinat for helpful discussions, the NSCCS for the supercomputer time, Alex D. Bain for providing a copy of the CIFIT-2 program and the Leverhulme Trust, and the ESPRC (EP/F065205,1,

EP/H003789/1) and the Universities of Durham, Manchester, and Oxford for support. N.M.K. thanks the Canon Collins Trust for his scholarship.

Supporting Information Available: Crystallographic data for L_{py} and its complexes in CIF format, crystal structure of the diprotonated ligand, $[H_2L_{py}][OTf]_2$, characterization data (including ^1H NMR spectra) for the Pr, Nd, Sm, Eu, Tb, and Dy complexes, COSY, EXSY, and HSQC NMR spectra of the Eu complex, variable-temperature ^{13}C NMR spectra (stacked plot) of the Eu complex, normalized steady-state optical emission spectra of the Tb, Sm, and Eu complexes, selected interatomic distances and angles for the Pr, Nd, Eu, Gd, Tb, Er, and Yb complexes, and a summary of the crystallographic data for the ligand, the diprotonated complex, and the Pr, Nd, Eu, Gd, Tb, Er, and Yb complexes. This material is available free of charge via the Internet at http://pubs.acs.org.